Computers and Chemical Engineering 124 (2019) 80–92

Contents lists available at ScienceDirect

Computers and Chemical Engineering

journal homepage: www.elsevier.com/locate/compchemeng

Stochastic back-off-based robust process design for continuous crystallization of ibuprofen

Xiangzhong Xie[a,b], René Schenkendorf[a,b,*]

[a] TU Braunschweig, Institute of Energy and Process Systems Engineering, Franz-Liszt-Straße 35, Braunschweig, 38106, Germany
[b] TU Braunschweig, Center of Pharmaceutical Engineering (PVZ), Franz-Liszt-Straße 35a, Braunschweig, 38106, Germany

ARTICLE INFO

Article history:
Received 12 December 2018
Revised 12 February 2019
Accepted 13 February 2019
Available online 15 February 2019

Keywords:
Back-off
Robust optimization
Polynomial chaos expansion
Uncertainty
Quality by design
Crystallization
Ibuprofen

ABSTRACT

Robust model-based process design in continuous pharmaceutical manufacturing aims to implement quality by design principles under uncertainty. Notably, various studies have discussed the back-off concept to solve the underlying robust optimization problem; however, for the concept to have practical value, its efficiency and convergence must be improved. In this work, we introduce a novel, highly efficient stochastic back-off strategy. Instead of using statistical moments of limited validity, we incorporate the full statistical information of the constraints to solve the robust process design problem. To ensure manageable computational costs, we make use of polynomial chaos expansion for uncertainty quantification and propagation. The proposed concept is demonstrated with the design of a tubular crystallizer for ibuprofen crystallization. The results show that the novel stochastic back-off strategy is considerably faster compared with the standard back-off concept and provides more reliable quality by design results in general.

1. Introduction

With the aim of efficiently and sustainably producing active pharmaceutical ingredients (APIs), concepts of quality by design (QbD) have been advocated by regulatory agencies in pharmaceutical manufacturing (ICH, 2005). In particular, continuous pharmaceutical manufacturing (CPM) has received keen interest in academia and industry over the last decade (Adamo et al., 2016; Mascia et al., 2013; Vervaet and Remon, 2005). Process analytical technology (PAT), which aims to design, analysis, and control the process, has been extensively explored and implemented in CPM to ensure consistent drug quality and safe operations (Simon et al., 2015; Zhang et al., 2014). Besides novel sensor concepts and measurement devices, mathematical models are considered as an essential tool for holistic PAT strategies to analyze critical quantities, to predict the process behavior, and to make decisions model-based results (Benyahia et al., 2012; Boukouvala et al., 2012; Cervera-Padrell et al., 2012; Gernaey et al., 2012; Gernaey and Gani, 2010; Jolliffe and Gerogiorgis, 2015; 2016; Lakerveld et al., 2013). However, the reliability of model-based results may suffer from uncertain model parameters that are typically derived from parameter identification routines processing noisy data (Maußner and Freund, 2018; Schenkendorf et al., 2018b). If these uncertainties are ignored, the model-based process design might lead to suboptimal performances and unexpected operation failures (Montes et al., 2018; Rooney and Biegler, 2003; Xie et al., 2018a; 2017). Therefore, it is necessary to include information about parameter uncertainties in the model-based design of pharmaceutical processes in general.

The robust design of pharmaceutical processes aims to maximize process performance while satisfying critical process constraints under the condition of uncertainty. A commonly used approach for robust optimization is the scenario-based method, in which simulation studies seek the worst-case scenario for which the process is optimized (Nagy and Braatz, 2003; 2004). However, the scenario-based method has two critical drawbacks: i) It leads to a complicated and intractable bilevel-optimization problem; ii) the worst-case scenario might rarely occur in reality, and thus, the derived robust solution is always too conservative. Alternatively, probability-based concepts provide less conservative robust process designs compared with the scenario-based method but increase the computational demand due to the inherent uncertainty propagation problem (Nagy and Braatz, 2007; Nagy, 2009; Telen et al., 2015; Xie et al., 2018a). Back-off terms, which are determined by the specified level of process robustness, are introduced to the inequality constraints to reduce their violation probability. For instance, Nagy and Braatz (2007) determined back-off terms with power series and polynomial chaos expansions in an

* Corresponding author at: TU Braunschweig, Franz-Liszt-Straße 35, 38106, Braunschweig, Germany
E-mail address: r.schenkendorf@tu-braunschweig.de (R. Schenkendorf).

https://doi.org/10.1016/j.compchemeng.2019.02.009
0098-1354/

analytical form with student's *t*-test distribution. Telen et al. (2015) calculated back-off terms with Cantelli's inequality and the unscented transform (Julier and Uhlmann, 2004). In both works, the back-off terms were updated in each iteration of the optimization. Although efficient methods were used to calculate the back-off terms, the computational cost might be prohibitive for problems with non-adequate optimization formulations, such as poor initial guesses.

There are at least two alternatives for applying the back-off concept to complex problems. To alleviate the computational burden for calculating back-off terms, a surrogate model could be used to replace the original process model as illustrated by Rafiei and Ricardez-Sandoval (2018); Rafiei-Shishavan et al. (2017); Schenkendorf et al. (2018a); Shen and Braatz (2016); Xie et al. (2017). The accuracy of the surrogate model, however, a crucial problem with this approach, especially for a large-scale optimization problem (Xie et al., 2017). Alternatively, Srinivasan et al. (2003) introduced an iterative strategy for calculating the back-off terms with superimposed optimization, so that robust optimization does not include additional complexity from calculating the back-off terms and has the same computational cost as solving the nominal optimization problem. Because of the computational efficiency, this approach has been further investigated and implemented in model-predictive control (Aydin et al., 2018), optimal experimental design (Galvanin et al., 2010), and robust process design (Emenike et al., 2019; Maußner and Freund, 2018; Shi et al., 2016).

In this work, we first summarize the structure of the conventional iterative back-off strategy briefly and improve the procedure by introducing a quantitative update rule for the back-off factor η that controls the conservativeness of a robust process design. Thus, the iterative back-off strategy can converge to the desired robustness for the given constraints without an intuitively selected η factor and its trial-and-error updating procedure, even for non-normal distributions. However, the two nested loops for determining back-off terms and the η factor introduce additional difficulties in the convergence of the conventional iterative back-off strategy. Moreover, the validation and calculation of the η factor limit the strategy's overall efficiency. Therefore, the main contribution of this work is to introduce a novel stochastic back-off strategy with a simpler structure. The key idea is that the back-off terms are derived by the entire probability distribution rather than the standard deviations of the constraints. Moreover, the efficiency of the stochastic back-off strategy is improved considerably by using polynomial chaos expansion to replace the CPU-intensive process model and to calculate the probability distributions of the constraints (Marelli and Sudret, 2015; Xiu and Karniadakis, 2002).

To demonstrate the performance of the stochastic back-off strategy, it is applied to continuous crystallization of ibuprofen. Ibuprofen is one of the most commonly used medicines for treating pain, fever, and inflammatory diseases. Continuous manufacturing of ibuprofen was investigated in Jolliffe and Gerogiorgis (2015); Montes et al. (2018), and the economic evaluation of this process was also provided in Jolliffe and Gerogiorgis (2016). Crystallization is the essential process in pharmaceutical manufacturing to extract APIs (Kwon et al., 2013; Montes et al., 2018; Nagy, 2009). In particular, the crystallization of ibuprofen was presented in Karunanithi et al. (2006); Nayhouse et al. (2015), in which the kinetic Monte Carlo method or group contribution method are used to predict the growth kinetic or solubility of ibuprofen in different solvent systems. Rashid (2011) identified the mechanisms and kinetics of the crystallization of ibuprofen in ethanol, e.g., the nucleation and growth rates, and estimated the associated kinetic parameters with experiments at various conditions. In our case study, the kinetics from Rashid (2011) are used to design a continuous tubular crystallizer for ibuprofen. The stochastic back-off strategy is implemented to ensure the solution supersaturation stays below the primary nucleation threshold to avoid unstable primary nucleation. Moreover, this strategy is compared with other iterative back-off strategies to highlight the superiority of the proposed concept in terms of efficiency.

The remainder of the paper is organized as follows. In Section 2, the basics of the traditional back-off strategy are presented. Next, our novel stochastic back-off strategy is introduced in Section 3. A case study involving the continuous crystallization of ibuprofen is detailed in Section 4. Results and discussions are provided in Section 5. Conclusions are given in Section 6.

2. Basics of the standard back-off strategy

Assume we have an inequality constraint for the process design

$$h(x,\theta) \leq 0, \tag{1}$$

where function $h : \mathbb{R}^{n_x \times n_\theta} \rightarrow \mathbb{R}^{n_h}$, x is the vector of the state variables, and θ is the vector of the uncertain parameters with the joint probability density function (PDF) $f(\theta)$. Technically, to ensure the robustness of the inequality constraint, Eq. (1) must be satisfied for all possible parameter realizations of PDF $f(\theta)$, but straightforward implementation of the equation results in a semi-infinite optimization problem that might be NP-hard. Thus, for *soft* inequality constraints Eq. (1), which might be violated with acceptable probability, we can introduce a back-off term b to ensure the reliability of the inequality constraint under uncertainty Xie et al. (2018a):

$$h(x,\theta_n) + b \leq 0, \tag{2}$$

where θ_n represents the vector of the nominal parameter values. Here, Eq. (2) has the same complexity as the inequality constraint for the nominal design, and the back-off term b, which could be a constant or time-varying variable, moves the inequality constraint at the nominal condition away from its boundary to ensure a sufficient safe distance for the parameter uncertainties.

Perkins et al.'s 1990 pioneering work on the back-off concept has been advanced to select control structures for different chemical processes, in which linearized models are used to calculate the back-off terms (Kookos and Perkins, 2016; Narraway and Perkins, 1993). The original back-off strategy has also been used to guarantee the dynamic feasibility of joint process design and control optimization problems (Bahri et al., 1995; 1996; Figueroa et al., 1996). Visser et al. (2000) and Diehl et al. (2006) approximated back-off terms with constraint derivatives for robust optimization of a fed-batch fermentation process and a batch distillation process, respectively. However, the back-off terms used were determined by linearization of the model and the constraints, and thus, are not reliable for the robust design of highly non-linear pharmaceutical processes and might lead to robustification that is too conservative or has excessive constraint violations. Moreover, Srinivasan et al. (2003) proposed the idea of an iterative calculation of back-off terms; i.e., in addition to the optimization loop, an outer back-off validation loop is used based on Monte Carlo simulations. This iterative back-off concept was also implemented and refined by Shi et al. (2016) for robust optimization of a polymerization process, in which Monte Carlo simulations were used to propagate the parameter uncertainties through the original process model and to approximate the resulting mean and variance values of the constraints for the back-off calculation as summarized in Eqs. (3) to (5):

$$b = \eta \sqrt{Var(h(x,\theta))}, \tag{3}$$

$$Var(h(x,\theta)) = \int_{I_\theta} (h(x,\theta) - \mathbb{E}(h(x,\theta)))^2 f(\theta) d\theta \tag{4}$$

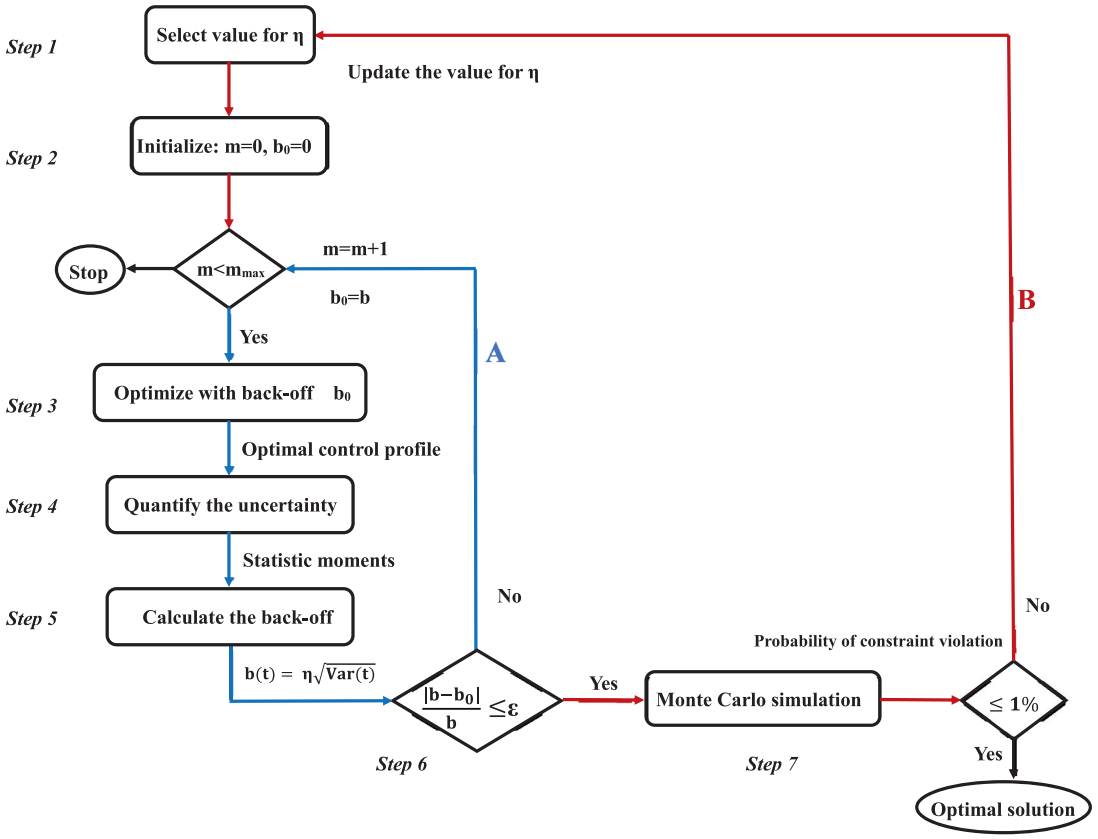

Fig. 1. Flow diagram for the double-loop back-off strategy for robust process design.

$$\approx \sum_{i=1}^{n_{MC}} \frac{1}{n_{MC}} (h(x,\theta_i^{MC}) - \mathbb{E}(h(x,\theta)))^2,$$

$$\mathbb{E}(h(x,\theta)) = \int_{I_\theta} h(x,\theta) f(\theta) d\theta \approx \sum_{i=1}^{n_{MC}} \frac{1}{n_{MC}} h(x,\theta_i^{MC}), \tag{5}$$

where n_{MC} is the number of Monte Carlo simulation samples, $\mathbb{E}(h(x,\theta))$ and $Var(h(x,\theta))$ indicate the mean and the variance of the constraint function h, and η is the factor that controls the conservativeness of the robust optimization using back-off terms. Shi et al. (2016) also demonstrated that we could improve the back-off terms with an iterative update based on Eqs. (3) to (5). The optimal design from the last iteration is used, and the results from the back-off strategy are equivalent to those from multi-scenario optimization once the back-off terms converge. To reliably approximate the mean and variance values with Eqs. (4) and (5), n_{MC} has to be large, which might be prohibitive especially for large-scale systems and complex process models. Emenike et al. (2019) came up with the idea of calculating back-off terms with the point estimate method (PEM) as a more efficient alternative to conventional Monte Carlo simulations and based on their simulation study, demonstrated a dramatic reduction in computational costs. In addition, Koller et al. (2018) investigated the impact of different η values on the performance of a back-off strategy by applying it to a simultaneous design, control, and scheduling problem of multi-product systems. Maußner and Freund (2018) introduced an additional iteration loop to update the η value to ensure that the number of constraint violations is below an acceptable level. This particular double-loop back-off strategy is summarized in the workflow diagram in Fig. 1.

The double-loop back-off strategy given in Fig. 1 has an internal loop (A) for the convergence of the back-off terms and an external loop (B) for updating the value of the η factor. More details about the double-loop back-off strategy presented in Emenike et al. (2019) are summarized below.

Step 1 (External loop (B) start)] Specify the initial η value. We take the quantile of the standard normal distribution with the desired probability. For example, we set the quantile equal to 2.33 to ensure that 99% of the inequality constraints are satisfied.

Step 2 Initialize the internal loop (A).

Step 3 (Internal loop (A) start) Optimize with the inequality constraints; i.e., $h(x,\theta) + b_0 \leq 0$, where b_0 is the back-off term. Note that the optimization in the first iteration with $b_0 = 0$ is equivalent to nominal optimization and has the same computational complexity as the nominal optimization problem in general.

Step 4 Quantify the impact of the parameter uncertainties on the constraints. The PEM is used to estimate the mean and variance of the constraints as given in Eqs. (6) and (7) based on the optimal design result from Step 3:

$$\mathbb{E}(h(x,\theta)) \approx \sum_{i=1}^{2n_\theta^2+1} w_i h(x,\theta_i^{PEM}), \tag{6}$$

$$Var(h(x,\theta)) \approx \sum_{i=1}^{2n_\theta^2+1} w_i (h(x,\theta_i^{PEM}) - \mathbb{E}(h(x,\theta)))^2, \tag{7}$$

where n_θ is the number of uncertain parameters, and w_i and θ_i^{PEM} are the weight factors and the deterministic parameter samples, respectively. (Xie et al., 2018a).

Step 5 Calculate the back-off terms with η and the variance calculated in Step 4 by using Eq. (3). We use the time-varying back-off terms $b(t)$ as it provides more flexibility and optimal results (Shi et al., 2016).

Step 6 **(Internal loop (A) end)** Check if the back-off terms converge; if not, we replace b_0 with the new back-off term b and repeat steps 3 to 6 until it converges.

Step 7 **(External loop (B) end)** With the converged back-off terms, we validate the optimal design with Monte Carlo simulations. To this end, we evaluate 10,000 realizations generated from the distribution of the parameter uncertainty and calculate the probability of a constraint violation. If the violation probability is smaller than 1%, we export the optimal solution. If not, we have to select a new value for η and repeat the whole algorithm. Note that any other violation probability might be feasible but affects the initial η value selection procedure in Step 1.

As we can see, the two loops are essential to fulfilling the probability of the given constraint violation limits. Note that the internal loop with the initial guess of η from the quantile of a standard normal distribution might be sufficient but only if the probability distribution of the constraint function follows a normal distribution. However, models for pharmaceutical processes are complex and highly nonlinear, and thus, the distribution of the constraint function is typically non-normal (Rossner et al., 2010). Maußner and Freund (2018) provided candidate values for η based on expert guessing to update the η factor. In this work, we propose a more systematic and problem-specific procedure for updating η according to:

$$\eta_i = \eta_{i-1} \frac{\text{norminv}(99\%)}{\text{norminv}(1 - e_c)}, \tag{8}$$

where norminv means the inverse cumulative density function of a standard normal distribution, and e_c is the probability of a constraint violation calculated in Step 7. This results in fewer η values needed to be tested, and thus, the overall efficiency of the double-loop back-off concept can be improved.

With the additional external loop, the double-loop back-off strategy is capable of handling constraints with non-normal distributions. However, the high computational costs and the redundant structure might be critical for many practical problems in robust process design. Although the PEM is used to reduce the cost of the internal loop considerably, the external loop still needs a vast number of Monte Carlo simulations to validate the probability of a constraint violation. For this reason, the computational efficiency of the double-loop back-off strategy deteriorates dramatically if the external loop converges slowly. To circumvent the redundant structure and the heavy computational burden for updating η, we propose a novel, highly effective stochastic back-off strategy.

3. The stochastic back-off strategy

Before we outline our novel approach, as a motivation, we explain why Eq. (3) is not an appropriate formulation for calculating the back-off terms first. In Fig. 2, we illustrate the calculation of back-off terms assuming a normal distribution (A) and a non-normal distribution (B). In particular, the back-off term b is determined with the distance between the nominal value of the inequality constraint and its 99% quantile. In the case of a normally distributed inequality constraint, the mean value is equal to the nominal value, and the back-off term b is equal to the confidence interval; i.e., $b = \eta_{99\%}\sqrt{Var(h(x,\theta))}$. However, in the case of a non-normal distribution, these two aspects do not hold, and thus, we have an external loop in the double-loop back-off

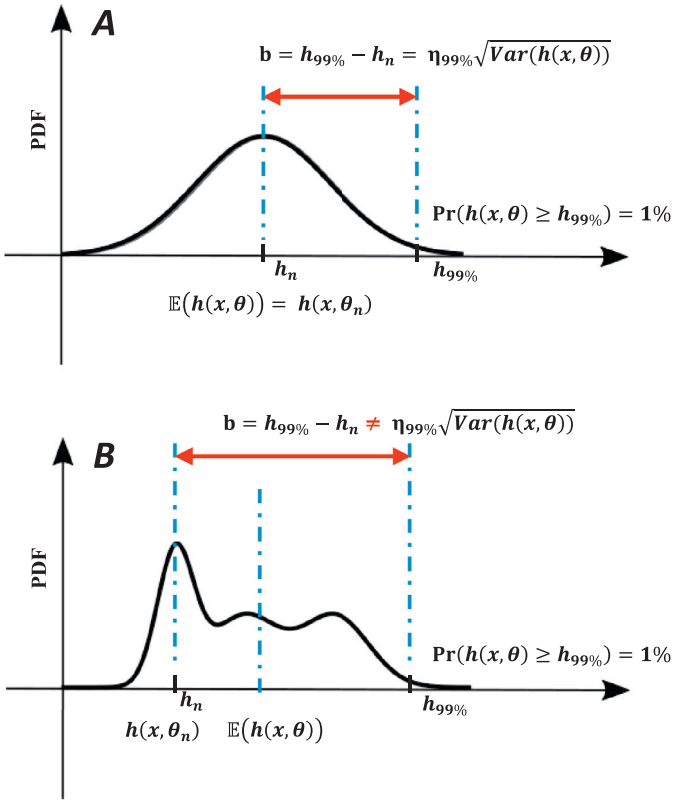

Fig. 2. Calculation of the back-off term, b, for the cases where the probability density function (PDF) of the constraint function $h(x, \theta)$ is normal (A) and non-normal (B) distributed. $h_n = h(x, \theta_n)$ and $h_{99\%}$ indicate the values of constraint function at the nominal point and the point with a cumulative density equal to 99%.

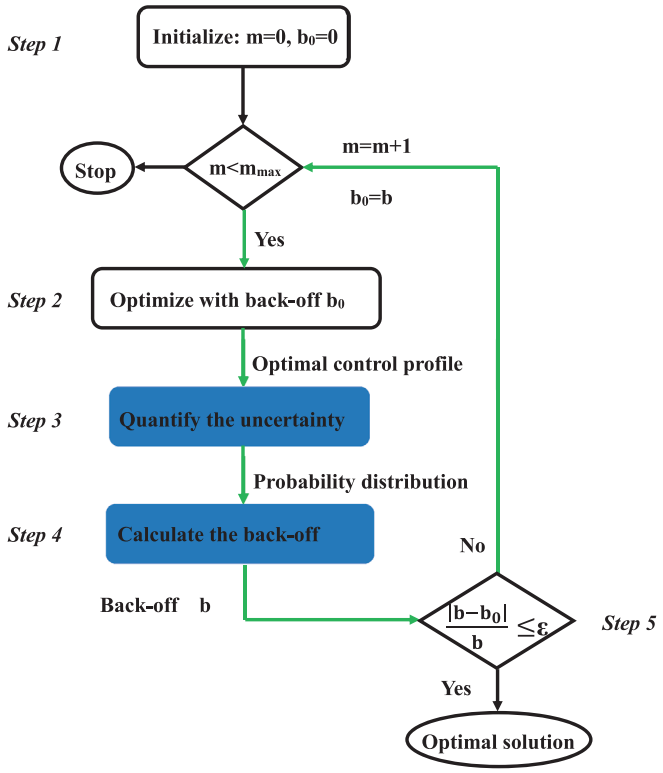

Fig. 3. Workflow of the stochastic (single-loop) back-off strategy for robust process design.

strategy to approximate the real value of the back-off terms by adapting the value of η iteratively; see Eq. (8). As mentioned, the iterative update of η is inefficient and might increase the computational cost dramatically. Alternatively, we suggest calculating the back-off term directly with the distance between its normal value and the empirical quantile at 99% without assuming a normal distribution. This key aspect is explained in more detail below.

In Fig. 3, we illustrate the workflow diagram of our novel stochastic back-off strategy. The structure of the stochastic back-off strategy is similar to the internal loop of the double-loops back-off strategy in Fig. 1 but has significant differences for the uncertainty quantification and the approximation of the back-off terms:

Step 1 (Loop start) Initialize of the stochastic back-off strategy.

Step 2 Optimize under inequality constraints; i.e., $h(x,\theta)+b_0 \leq 0$. Note that the optimization in the first iteration with $b_0 = 0$ is actually equivalent to nominal optimization, and thus, has the same computational complexity as nominal optimization.

Step 3 Propagate and quantify the constraint uncertainties with the optimal design from Step 2 Instead of the variance, the exact shape of the probability distribution of the constraints is approximated with the kernel density estimator (KDE) and polynomial chaos expansion. The KDE is a non-parametric method for estimating the probability density function of random variables with an arbitrary probability distribution (Epanechnikov, 1969) according to:

$$\hat{f}(h) = \frac{1}{n\Delta}\sum_{i=1}^{n} K\left(\frac{h-h_i}{\Delta}\right), \tag{9}$$

where n is the number of samples, K is the kernel function, and Δ is the bandwidth. h_i is the constraint evaluation at sample i.

To avoid a repetitive evaluation of the original CPU-intensive model, we propose the polynomial chaos expansion (PCE) approach as an alternative concept. Thus, the original process model is replaced by a surrogate model that can be evaluated with low computational costs (Isukapalli et al., 1998; Kim and Braatz, 2013; Kim et al., 2013; Nagy and Braatz, 2007; Xie et al., 2017). When the PCE approach is used, the original process model is approximated with an empirical polynomial model:

$$h(x(t),\boldsymbol{\theta}) = \sum_{k=0,1,2,\ldots} \alpha_k(t)\Psi_k(\boldsymbol{\theta}), \tag{10}$$

where $\Psi_k(\boldsymbol{\theta})$ and $\alpha_k(t)$ are the polynomial basis and corresponding time-varying coefficients, respectively. Blatman and Sudret (2011) presented the detailed procedure for efficiently constructing the polynomial basis and estimating the coefficients of the PCE model. A small number of samples, which are generated from the probability distribution of the uncertain model parameters, are evaluated with the original model. Based on these model evaluations, the corresponding values of the constraints are calculated and used as references to identify the coefficients for the PCE model. Note that all samples in this work are generated with a quasi-random low discrepancy sequence, also known as Sobol' sequence. Moreover, the PCE model specifications, e.g., the maximum order of the polynomial basis, type of truncation, etc., are selected a prior according to Marelli and Sudret's 2015 guidance. The basis functions are derived from the Wiener–Askey scheme (Xiu and Karniadakis, 2002) for the parameters of specific distributions or with the Stieltjes procedure (Gautschi, 2004) for the parameters with empirical distributions. Then, the coefficients $a_k(t)$ are estimated by fitting the collected evaluation values with the PCE model in Eq. (10) via the least angle regression method (Efron et al., 2004; Xie et al., 2017). The number of samples for estimating the PCE model depends on the complexity of the model and the number of uncertain parameters but is typically negligible compared to the number of samples needed for approximating the probability distribution. For models with a large number of uncertain parameters, global sensitivity analysis techniques can be implemented to quantitatively determine the importance of parameter uncertainties on model outputs, e.g., state variables and their constraints (Saltelli et al., 2005; Xie et al., 2018b). Based on the sensitivity analysis, parameter uncertainties with considerable influence are taken into account, while the rest are neglected to improve the efficiency of the uncertainty propagation further. Moreover, process noise, which accounts for model uncertainties and model-plant mismatch, could also be incorporated within the robustification framework (Mandur and Budman, 2014; Paulson and Mesbah, 2017; Savin and Faverjon, 2017).

Note that Monte Carlo simulations as a traditional sample-based method could also be used here for the uncertainty quantification step. However, the deficiency of Monte Carlo simulations, as was addressed in the double-loop approach (Emenike et al., 2019), might be prohibitive for the stochastic approach.

Step 4 Calculate of the back-off terms with the probability distribution of the constraints. As shown in Fig. 4, the sample evaluations from the PCE model are processed to approximate the probability distribution of the constraint function making use of the KDE. The resulting probability distribution is subsequently used to calculate the back-off term. As illustrated in Fig. 2, it is more appropriate to calculate the back-off terms with the empirical quantile distance than just the standard deviation. Therefore, the back-off terms for robust design with a probability of a constraint violation of $\leq 1\%$ are determined by:

$$b = D(h_n, h_{99\%}) = \hat{F}_h^{-1}(99\%) - h_n, \tag{11}$$

where $D(\cdot)$ means the distance function, and $\hat{F}_h^{-1}(\cdot)$ is the inverse cumulative density function of the constraints adapted from Eq. (9).

Note that the probability distribution of model outputs could also be approximated with statistical moments, which can be analytically determined with the coefficients of the PCE. However,

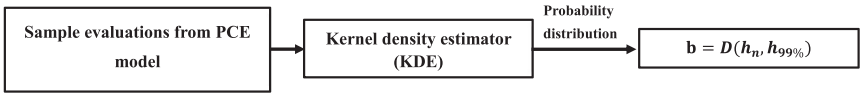

Fig. 4. Calculation of the back-off term, b, for the stochastic back-off strategy. $D(h_n, h_{99\%})$ is the distance function that calculates the difference between h_n and $h_{99\%}$. h_n and $h_{99\%}$ indicate the values of the constraint function at the nominal point and the point with a cumulative density equal to 99%, respectively.

only the first two statistical moments, i.e., the mean and the variance, have the analytical form while higher-order statistical moments might fail (Savin and Faverjon, 2017). Moreover, non-normal distribution cannot be characterized with only the first two statistical moments. Therefore, KDE in combination with PCE is a proper choice in this case.

Step 5 (Loop end) Check if the back-off terms converge. If not, we replace b_0 with the new back-off b and repeat steps 2 to 5 until the procedure converges.

To conclude, the novel concept of a stochastic back-off implementation has a simpler structure in comparison to the double-loop back-off strategy while PCE ensures low computational costs at the same time. More details about the performance of the novel stochastic back-off concept are described in the following case study.

4. Case study: a continuous tubular crystallizer for ibuprofen

The case study aims to design a continuous tubular crystallizer for the API ibuprofen. The tubular crystallizer has the advantage of higher efficiency and narrower crystal distributions compared with the commonly used mixed suspension mixed product removal crystallizer (MSMPRC) and has been used to crystallize various APIs (Eder et al., 2010; Su et al., 2015). The focus of this work is to optimize the steady-state operation of the tubular crystallizer and to maximize the mass-based mean crystal size (d_{43}) under the condition of uncertainty.

4.1. Mathematical model

The scheme of a continuous tubular crystallizer is illustrated in Fig. 5. The model for the tubular crystallizer consists of the population balance equation (Eq. (12)) that describes the evolution of the crystal size distribution (CSD) and the mass balance equation (Eq. (13)) that describes the mass balance in the liquid and solid phases. Note that we assume no dissolution, agglomeration, and breakage happen for the crystallization of ibuprofen as discussed in Rashid (2011). We also assume that no mixing effect exists in the tubular crystallizer, dispersions of the crystal density and the API concentration exist only in the axis direction, and the flow velocity is constant across all the cross-sections perpendicular to the axis of the pipe (e.g., plug flow condition). The governing equations for the steady-state tubular crystallizer model are:

$$0 = \frac{\partial(vn)}{\partial z} + \frac{\partial(Gn)}{\partial L}, \tag{12}$$

$$\text{Liquid:} \quad 0 = \frac{\partial vC}{\partial z} + k_v \rho_s \left(BL_0^3 + 3 \int_0^\infty GL^2 n dL \right), \tag{13}$$

where z is the axis coordinate of tubular crystallizer, m; L is the characteristic crystal size, m; n is the population density of crystals per kilogram of slurry, #/kg/m; B is the nucleation rate, #/kg/s; G is the crystal growth rate, m/s; C is the mass of solute per kilogram slurry, kg/kg; k_v and ρ_s are the shape factor and the density of the crystals, kg/m^3, respectively, and v is the superficial velocity of the slurry along the tubular crystallizer, m/s. The mass of the solution and the solids is considered, and we assume that the formation of the solids does not change the volume of the slurry. Therefore, the superficial velocity v is considered as constant for the entire tubular crystallizer. Note that the mass equation for the solid phase is already implicitly included in Eq. (12). The boundary conditions at $z = 0$ and $L = L_0$, where L_0 is the size of the nuclei, m, of the model are:

$$n(0, L) = n_{feed}(L), \tag{14}$$

$$n(z, L_0) = \frac{B}{G}, \tag{15}$$

$$C(0) = C_{feed}, \tag{16}$$

where n_{feed} and C_{feed} are the CSD of seeds and the concentration of solute in the feed. Note that seeded feed is only used at the start-up of the crystallization process (Su et al., 2015). For the steady state that we are interested in this work, only the unseeded solution is fed to the crystallizer, and the secondary nucleation then happens with existing crystals.

As we can see, the steady-state tubular crystallizer model consists of partial differential equations (PDEs) and has to be discretized or modified to be solved by a common ordinary differential equation (ODE) solver. The classical method of moments (MOM) can be used to transfer the PDEs into several ODEs because the growth rates G are size independent (Rashid, 2011; Su et al., 2015). For the classical MOM, size density n is multiplied with the k^{th} order of crystal size L and subsequently integrated over the entire crystal size domain to compute its k^{th} moment, i.e, μ_k. Typically, the first sixth moments, $k = 0, \ldots, 5$, are used to represent

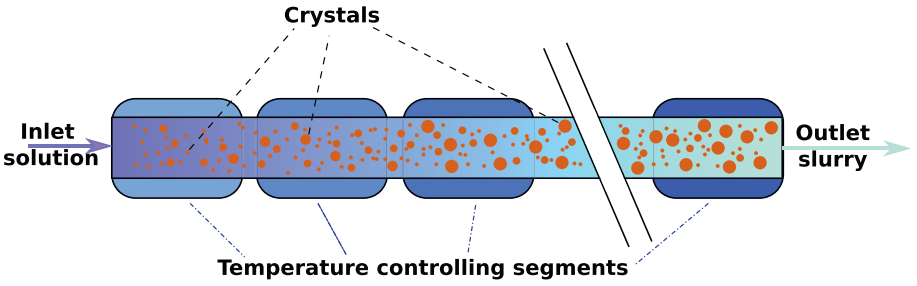

Fig. 5. Scheme of the continuous tubular crystallizer for ibuprofen. The temperature controlling segments are used to realize an optimal temperature profile for the crystallizer.

the key information included in size density n:

$$\mu_k = \int_0^\infty L^k n dL, \quad k = 0, \ldots, 5. \tag{17}$$

The resulting ODE system and initial conditions read as:

$$\frac{d\mu_0}{dz} = \frac{B}{v}, \tag{18}$$

$$\frac{d\mu_k}{dz} = \frac{BL_0^k}{v} + \frac{kG\mu_{k-1}}{v} \quad k = 1, \ldots, 5, \tag{19}$$

$$\text{Liquid:} \quad \frac{\partial C}{\partial z} = -\frac{k_v \rho_s}{v}(BL_0^3 + 3G\mu_2), \tag{20}$$

$$\mu_k(0) = \int_0^\infty L^k n_{feed} dL, \quad k = 0, \ldots, 5, \tag{21}$$

where $\mu_k(0), \quad k = 0, \ldots, 5$ are the initial conditions for the moment equations. Alternatively, to calculate the probability density of the crystal number, a high-resolution scheme based on the finite-volume method (FVM) is used to solve the PDEs with the discretization of the characteristic crystal length L. The resulting ODEs are given in Eq. (22) that could be solved directly with Eq. (13) with standard ODE solvers to calculate the probability density of the crystal number. The cell-face fluxes $n_{L_{i\pm1/2}}$ are computed with a robust upwind discretization method (Qamar et al., 2006):

$$\frac{\partial (n_i)}{\partial z} + \frac{G}{v\Delta L}(n_{L_{i+1/2}} - n_{L_{i-1/2}}) = 0, \quad i = 1, \ldots, N. \tag{22}$$

The classical MOM generates less complex ODE systems ($= 7$), and therefore, is more suitable for the optimal (robust) crystallizer design regarding the computational costs. In contrast, the FVM needs a fine mesh (≥ 100) for the characteristic crystal length and is too redundant to be embedded in the optimization algorithm. Therefore, we use the FVM only to generate the reference probability density of the crystal number for illustration and validation in what follows.

4.2. Crystallization kinetics of ibuprofen

The kinetics for the crystallization of ibuprofen in absolute ethanol are adapted from Rashid's 2011 work. The main driving force for crystallization is the degree of supersaturation S, which is defined with the difference between solution concentration C_{sol} and solubility C^* as:

$$S(z) = C_{sol}(z) - C^*(T(z)). \tag{23}$$

The solubility of ibuprofen in absolute ethanol is a function of the temperature, and thus, can be used to design the crystallization process:

$$C^* = 0.495 + 0.001026T^2. \tag{24}$$

All the quantities above have the same unit kilogram of solute per kilogram of ethanol. The concentration of the solution can be derived from the slurry mass solution C and the solid concentration C_s with the following relations:

$$C_{sol} = \frac{C}{1 - C - C_s} \tag{25}$$

$$C_s = k_v \rho_s \mu_3. \tag{26}$$

Technically, the solubility of ibuprofen changes not only with the temperature but also with the composition of the solution. Water as an antisolvent can be added to decrease the solubility of ibuprofen as investigated by Rashid (2011). However, ibuprofen induces phase separation in the water-ethanol mixture especially at 40°C (Rashid, 2011). Moreover, the information about ibuprofen solubility in the water-ethanol mixture is not complete. Therefore, we only focus on the crystallization of ibuprofen in absolute ethanol. The kinetics for crystallization, i.e., the nucleation rate and the growth rate, in absolute ethanol are given below, and the values for the kinetic parameters in Eqs. (27) and (28) are listed in Table 1:

Table 1
Nominal values and units of the parameters for ibuprofen crystallization and the tubular crystallizer.

Parameters	Unit	Nominal value
k_{b_0}	#/kg/s/(kg solute/kg ethanol)	1.73×10^8
k_{g_0}	m/s/(kg solute/kg ethanol)	5.3
T_g	°C	42
n_b	-	1
n_g	-	1
k_v	-	$\pi/6$
ρ_s	kg/m^3	1100
v	m/s	0.007
z_f	m	20.16

$$B = k_{b_0} S^{n_b} \tag{27}$$

$$G = k_{g_0} \exp\left(\frac{T}{T_g}\right) S^{n_g}. \tag{28}$$

4.3. Optimization problem

In this section, the structure of the nominal optimization problem of the tubular crystallizer is introduced in Eq. (29). The objective function in Eq. (29a) is to maximize the critical quality attribute (*CQA*) of the crystallization process, i.e., the mass-based mean crystal size d_{43} at the outlet of the tubular crystallizer. The MOM implementation of the tubular crystallizer model and the kinetics of ibuprofen crystallization are used in Eq. (29b) to calculate the objective function and the constraints of the optimization problem. There are three inequality constraints and one equality constraint included in the optimization problem. The first inequality constraint, Eq. (29c), ensures that supersaturation S is within the metastable zone to avoid primary nucleation. This inequality constraint is important for two reasons: i) only the kinetics of secondary nucleation is provided by Rashid (2011), and ii) the primary nucleation, which is a spontaneous process that happens in the region above the primary nucleation threshold (*PNT*) in the phase diagram as discussed by Rashid (2011). Primary nucleation is commonly avoided in industrial operations because it restrains the growth of crystals by creating a huge number of fine crystals and is unstable. Moreover, the *PNT* measured by Rashid (2011) is used here. The second inequality constraint, Eq. (29d), ensures the yield of the crystallization process is above 95%. The third inequality constraint, Eq. (29e), avoids temperature increase as we do not include the kinetics for dissolution in the model. The equality constraint Eq. (29f), in turn, calculates the value of d_{43} as the objective function. The tubular crystallizer consists of 20 temperature controlling segments, where each segment is almost 1 m long, and the temperature of each segment is bounded within the range where the solubility information is available, i.e., Eq. (29g) is fulfilled.

$$\min_{\mathbf{T}(\cdot)} \quad -d_{43}(z_f), \tag{29a}$$

subject to:

$$\text{Mathemical model:} \quad \text{Eqs. (18) to (20), (23) to (28)} \tag{29b}$$

$$\text{Inequality constraints:} \quad \frac{S(z)}{C^*(T(z))} \leq PNT \quad \forall z \in [0, z_f] \tag{29c}$$

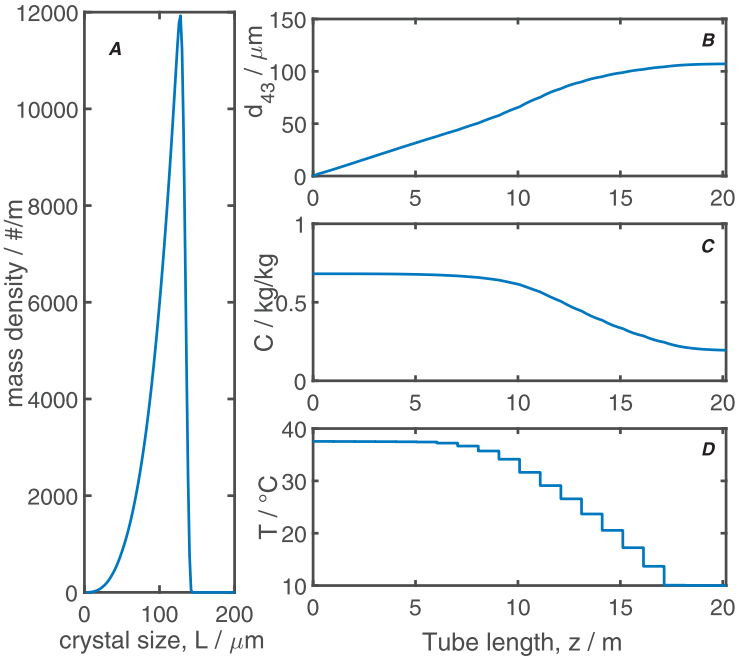

Fig. 6. Results from the nominal design of the tubular crystallizer. ***A*** is the mass-based crystal size distribution (CSD) at the tubular crystallizer outlet. ***B, C***, and ***D*** are the evolution profiles of the mass-based mean crystal size (d_{43}), the mass concentration of solute ibuprofen (C), and the operation temperature along the tubular crystallizer axis, respectively.

$$\frac{C(0)-C(z_f)}{C(0)-C^*(10^\circ C)} \geq 95\% \tag{29d}$$

$$\frac{dT(z)}{dz} \leq 0 \quad \forall z \in [0, z_f] \tag{29e}$$

$$\text{Equality constraints:} \qquad d_{43}(z_f) = \frac{\mu_4(z_f)}{\mu_3(z_f)} \tag{29f}$$

$$\text{Bounds:} \qquad 10^\circ C \leq T(z) \leq 40^\circ C \quad \forall z \in [0, z_f] \tag{29g}$$

The case study is coded in MATLAB®(Version 2017b, The MathWorks Inc., Natick, Massachusetts, USA). The tubular crystallizer model and the optimization problem are solved by using the functions *ode*15*s* and *fmincon*, respectively. For all optimization results, we used a multi-start strategy to avoid local optima. The polynomial chaos expansion model is built with UQLaB (Version 1.0, ETH Zurich, Switzerland).

5. Results and discussion

First, the results of the nominal design are discussed. Then, the adverse effects of the parameter uncertainties on the nominal process design are shown. To alleviate the influence of parameter uncertainties, the stochastic back-off strategy is then used for the robust design of the tubular crystallizer. The double-loop back-off strategy and the stochastic back-off strategy using Monte Carlo simulations are also implemented as references. Finally, the convergence and computational demands of the different approaches are compared.

5.1. Nominal design

The saturated solution of ibuprofen in pure ethanol at 40°C is fed into the tubular crystallizer with a total length of $z_f = 20.16$ m. The optimal temperature profile for the tubular crystallizer, which includes 20 controlling segments, is derived by solving the nominal optimization problem given in Eq. (29). Results derived from the nominal design are depicted in Fig. 6. On the left side of Fig. 6 we show the complete mass-based CSD at the reactor position $z_f = 20.16$ that was derived from Eq. (22) with $N = 100$. On the right side of Fig. 6, we illustrate the evolution profiles of d_{43}, solution concentration C, and temperature T along the axis of the crystallizer. To gain a better understanding of the results from the nominal design, we have to consider the supersaturation profile given in Fig. 7. The first part of the tubular crystallizer has a relatively high reactor temperature and low supersaturation; i.e., fewer nuclei are generated, and the growth rate is maintained at a comparatively high value as indicated by the slope of the curve in Fig. 6B. Consequently, the consumption of ibuprofen in solution is also low, and solute concentration C does not decrease too much

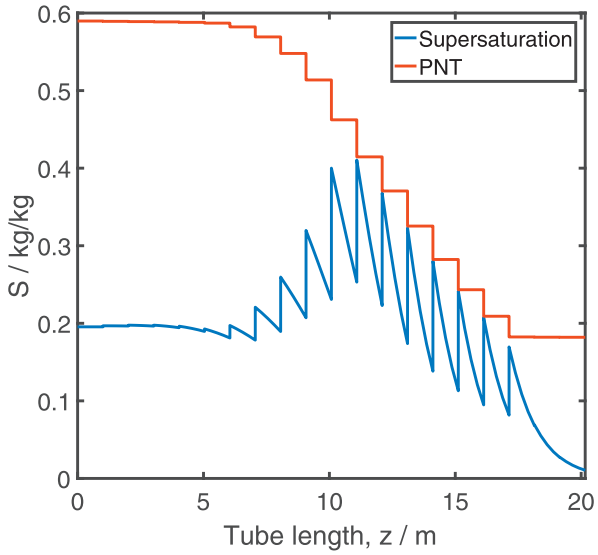

Fig. 7. Profile of supersaturation (S) along the axis of the tubular crystallizer. *PNT* is the primary nucleation threshold.

Table 2
Uncertainties and feasible ranges of the kinetic parameters based on Rashid (2011).

Parameters	Uncertainty	Range
k_{b_0}	$\mathcal{N}(1.73 \times 10^8, 2.6 \times 10^7)$	$[0, \infty]$
k_{g_0}	$\mathcal{N}(5.3, 0.69)$	$[0, \infty]$
T_g	$\mathcal{N}(42, 12.6)$	[20,65]

at the beginning. However, to achieve the desired yield at the end of the tubular crystallizer, the temperature decreases gradually at higher amplitudes, and the supersaturation increases to its upper limit. As a result, the consumption of ibuprofen in the solution is increased. The predicted yield at the end of the tubular crystallizer is 99.31%. With the nominal design, the final mass-based mean crystal size is maximized while all given constraints are satisfied. We also calculated another important CQA for the crystallization process, i.e, the coefficient of variation (*CV*) of the crystal size distribution according to Eq. (30). The CV value for the tubular crystallizer is equal to 0.21, which is much smaller than 0.5 for a single-stage MSMPRC, and reveals another important benefit of the tubular crystallizer. In principle, the CV could also be used directly as an objective function, but that is beyond the scope of this work.

$$CV = \sqrt{\frac{\mu_5 \mu_3}{\mu_4^2} - 1} \tag{30}$$

5.2. Effect of parameter uncertainties on the nominal design

According to Rashid's 2011 study, experimental data of the crystallization process are considerably affected by measurement noise and environmental conditions. The resulting data uncertainties lead to strong deviations in the estimation of the kinetic parameters for the nucleation and growth rates. Based on the estimated kinetic parameters and their confidence intervals (CIs) from Rashid (2011), we summarized the parameter uncertainties of k_{b_0}, k_{g_0}, and T_g in Table 2 assuming normal density distributions. Samples of the kinetic parameters are generated based on the assigned probability distributions, and simulations of the tubular crystallizer model with the generated samples and the nominal optimal solution are conducted to analyze the influence of the parameter uncertainties on the constraints. Note that only the *soft* constraints, i.e., the inequality constraints in Eqs. (29c) and (29d), are affected by the parameter uncertainties as explained by Rangavajhala et al. (2007). In Fig. 8a, we show the evolution profile of the supersaturation and its 99% CI along with the tubular crystallizer axis. When considering parameter uncertainties, the supersaturation exceeds the *PNT* with a comparatively high probability. In other words, the inequality constraint in Eqs. (29c) might be violated, and thus, lead to undesired primary nucleation. Fig. 8b presents the probability distribution of the yield of the tubular crystallizer. The value of the yield also varies due to the parameter uncertainties, but the corresponding inequality constraint is still satisfied for all realizations. Thus, in this work, we focus on designing a tubular crystallizer under the condition of parameter uncertainties, so that the supersaturation does not exceed the *PNT*.

5.3. Robust design with the stochastic back-off strategy

Robust optimization has the same structure as the nominal optimization in Eq. (29), except that the back-off terms are added to the inequality constraint in Eq. (29c) as:

$$S(z) + b(z) \leq PNT \times C^*(T(z)) \quad \forall z \in [0, z_f], \tag{31}$$

in which the value of back-off terms $b(z)$ depends on the position in the tubular crystallizer. In doing so, we ensure that the supersaturation does not exceed the *PNT* in the presence of parameter uncertainties.

The stochastic back-off strategy introduced in Section 3 is then used to solve the robust optimization problem. The maximum iteration number $m_{\max}$ is set to 10, the desired violation probability of the inequality constraints is set to 1%, and the convergence criterion ε to calculate back-off terms is set to 0.02. For the PCE model, the polynomial basis is constructed with the Stieltjes procedure, as the boundaries on the parameter uncertainties change the structure of the distribution. The full set of the polynomial basis is truncated to the maximum order of 7, and 100 samples are used to estimate the PCE coefficients. For the KDE, a Gaussian kernel is assumed, an optimal bandwidth is determined (Botev et al., 2010), and 10,000 samples are used, respectively. Note that these 10,000 samples are evaluated with the PCE model, and thus, the computational costs of the KDE are negligible. The optimized temperature profile is depicted and compared with the result from the nominal design in Fig. 9. As we can see, the temperature profile of the robust design is lower than that from the nominal design for the first half of the tubular crystallizer and higher for the second half of the tubular crystallizer to compensate the effect of the parameter uncertainties on the inequality constraint for supersaturation. Note that the lower temperature induces also higher supersaturation in the first half of the tubular crystallizer when implementing

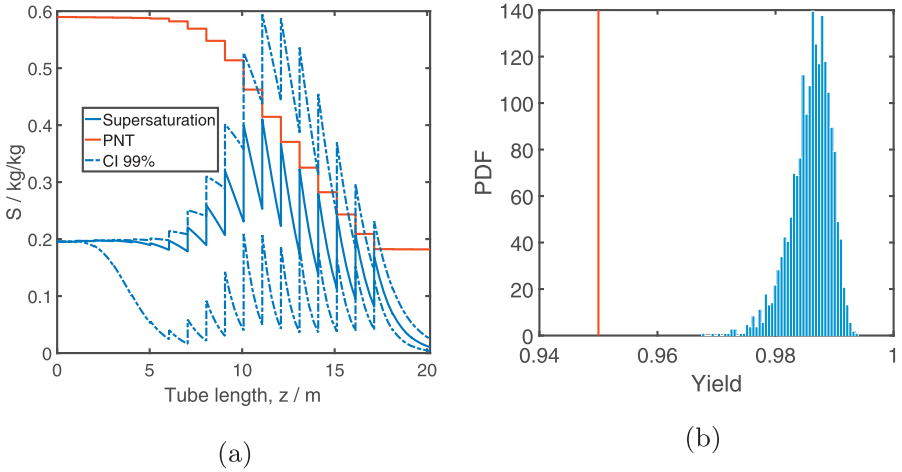

Fig. 8. (a) Profile of supersaturation (S) and its 99% confidence interval (CI) along the axis of the tubular crystallizer. *PNT* is the primary nucleation threshold. (b) The probability density function (PDF) of the yield.

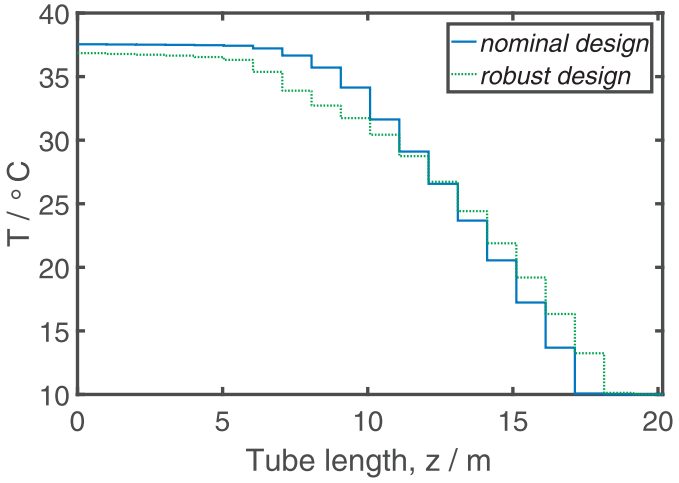

Fig. 9. The operation temperature profiles from the nominal and robust designs.

the robust design. From a practical point of view, this might cause severe side effects, e.g., clogging effects in the crystallizer. Naturally, additional constraints lowering the risk of malfunction and high maintenance costs could be included in the mathematical optimization problem (Eq. 29(a–g)) but is out of the scope of this work.

In Fig. 10, we further analyze the results of the inequality constraints from the robust design. By comparing the supersaturation profiles given in Fig. 10a and 8a, we can see that the mean value of the supersaturation in the first half of the tubular crystallizer is a bit higher than that from the nominal case. The robust design attempts to consume more ibuprofen solute and to generate more nuclei in the first half which lowers the supersaturation in the second half of the crystallizer. By doing so, the 99% CI of the supersaturation from the robust design is perfectly below the *PNT*. Moreover, the corresponding back-off terms are illustrated in Fig. 10b. The magnitude of the back-off terms varies considerably along the tubular crystallizer axis. Thus, the "time-varying" back-off term is more preferable than the constant back-off term in this study as the time-varying term provides more flexibility in the robust design.

5.4. Comparison of the different back-off strategies

In what follows, three different back-off strategies are compared in terms of their performance and efficiency. For the sake of readability, the double-loop back-off strategy is labeled *dlboPEM* as the PEM is used to calculate the back-off terms. The proposed stochastic back-off strategy is labeled *sboPCE*. The stochastic back-off strategy, in turn, where Monte Carlo simulations are used for calculating the back-off terms is labeled *sboMCs* and serves as the reference. The general setting of the optimization problem has not been changed; i.e., $m_{\max}$, the desired violation probability, and the convergence criteria are the same as in the previous section.

First, the convergence results are depicted and compared in Fig. 11. The convergence of the internal and external loops for *dlboPEM* is shown in Fig. 11a. The back-off terms converge after the first external iteration, but the desired probability of the constraint violations is not satisfied. Thus a second external iteration is required. Within the second external iteration, Eq. (8) is used to update the η value which leads to the specified performance of the robust tubular crystallizer design. The proposed update concept (Eq. (8)) ensures a target-oriented and systematic correction of the η value, which is much more efficient than in those studies where different values for η are tested heuristically (Koller et al., 2018; Maußner and Freund, 2018). For stochastic back-off strategies, there is only one iteration loop. The convergence results for the single loop of *sboMCs* and *sboPCE* are shown in Fig. 11b and c, respectively. *sboMCs* and *sboPCE* converge with a similar trend as they differ only in the detail of uncertainty propagation, i.e., the use of Monte Carlo simulations or the PCE. *sboMCs* requires more iteration steps than *sboPCE*, which might be due to the randomness of the samples. The convergence plots in Fig. 11 reveal that all three approaches can ultimately converge to a robust solution. The operation temperature profiles obtained from the three back-off strategies are compared in Fig. 12. The temperature profiles are almost identical. Thus, all three robustification concepts that make use of the back-off strategy to converge to the same robust solution. Table 3 lists more details about the tubular crystallizer performance, i.e., the $\mathbb{E}(d_{43})$, the violation probability, and the computational costs for the different back-off strategies. The same quantities for the nominal design are also listed for the sake of completeness. Please note that the violation probability in Table 3 is only for the inequality constraint in Eq. (29c), and the computational costs

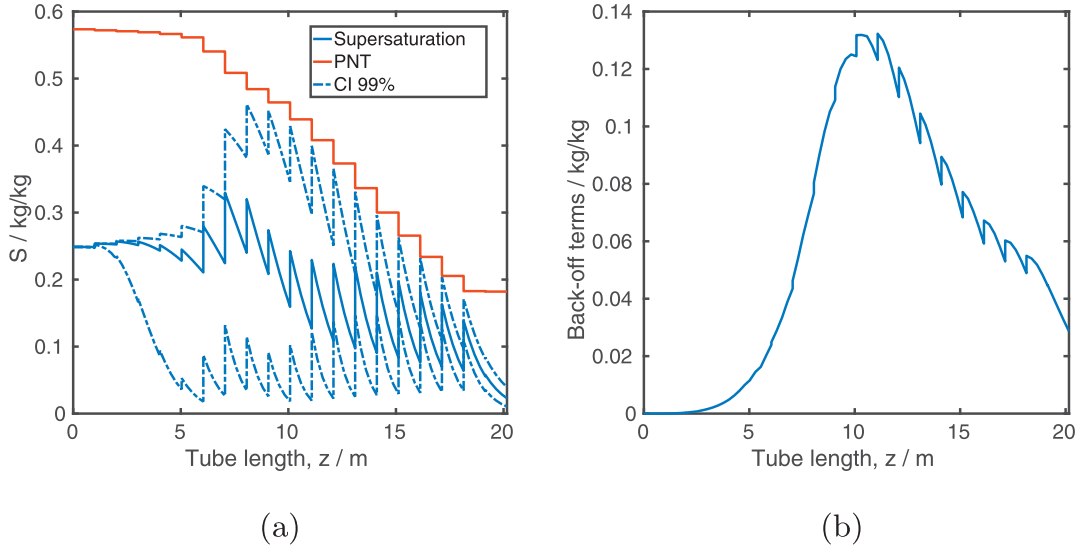

Fig. 10. (a) Profile of supersaturation (S) and its 99% confidence interval (CI) and (b) profiles of the back-off terms along the axis of the tubular crystallizer. *PNT* is the primary nucleation threshold. Results are from the robust design of the tubular crystallizer with the stochastic back-off strategy based on polynomial chaos expansion.

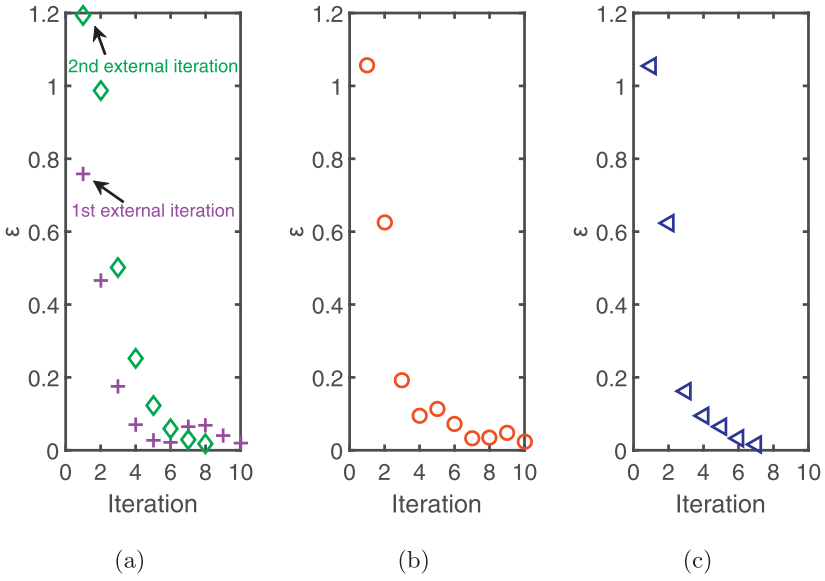

Fig. 11. The convergence rates of the back-off values for (a) *dlboPEM*, (b) *sboMCs*, and (c) *sboPCE*.

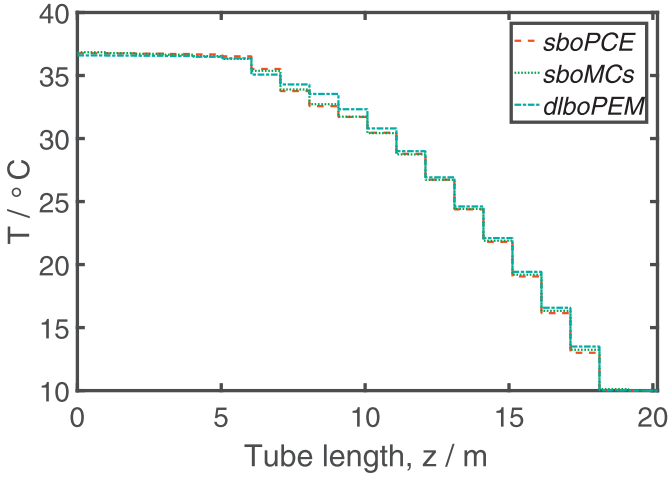

Fig. 12. The operation temperature profiles from the nominal and robust designs.

Table 3
Results of the mean value of the mass-based mean crystal size ($\mathbb{E}(d_{43})$), the violation probability from 10,000 realizations, and computational costs with respect to the number of model evaluations.

Approaches	$\mathbb{E}(d_{43})$	Violation probability	Needed reference simulations
Nominal	109.3	48%	0
dlboPEM(1st iter)	108.8	3%	10,190
dlboPEM(2nd iter)	108.6	1.1%	20,342
sboMCs	108.7	1.2%	100000
sboPCE	108.7	0.9%	700

reflect the model evaluation time of the original crystallizer model to calculate the back-off terms. The data in Table 3 are derived based on 10,000 realizations with the original tubular crystallizer model. Results from the nominal design have the maximum $\mathbb{E}(d_{43})$ value, but the violation probability, 48%, is much higher than the given specification of 1%. In contrast, the results from the robust designs have much lower violation probabilities, which are close to the desired value of 1%, while there is only a slight performance loss of $\mathbb{E}(d_{43})$. For the *dlboPEM* implementation, the violation probability is almost three times higher than the desired value after the first external iteration and reduces to almost 1% after the second external iteration. The violation probabilities from the robust design with *sboMCs* and *sboPCE* are close to 1% after the first external iteration. This proves that the simpler structure of the proposed stochastic back-off strategy does not need additional CPU-intensive loop iterations to ensure the desired robustness in the inequality constraints. Moreover, *sboPCE* has the highest efficiency, which is more than 20 times faster than *dlboPEM* and *sboMCs*. In summary, all three back-off strategies can guarantee the robustness of the inequality constraints in the design of a tubular crystallizer under parameter uncertainties. However, the PCE-based stochastic back-off strategy (*sboPCE*) has the best computational efficiency, and thus, it shows the perfect balance of process performance, robustness, and computational demand.

6. Conclusions

To guarantee reliable results in model-based process design, effective robustification concepts must be applied. For instance, the iterative back-off strategy proposed by Srinivasan et al. (2003) has received keen interests in academia and industry and has been implemented in various studies in robust optimization. In this work, we improved the original procedure and proposed a novel stochastic back-off strategy with two key benefits: 1) a simpler structure and 2) higher efficiency. The stochastic back-off strategy calculates back-off terms with a distance function based on the probability distribution of the constraints. The performance of the conventional back-off approach and the stochastic back-off approach were studied for the crystallization of ibuprofen within a tubular crystallizer. To this end, we implemented the nominal process design and then analyzed the adverse effects of the parameter uncertainties. If we ignore the parameter uncertainties in the design phase aiming for the highest mass-based mean crystal size, an optimized temperature profile was derived which, most likely, causes extreme supersaturation and constraint violations. Alternatively, we successfully demonstrated that the stochastic back-off approach results in a temperature profile that shows the perfect balance of process performance and robustness, i.e., a high mass-based mean crystal size and constraint violations within the given specification. Next, a detailed analysis of the computational costs and practical implementation aspects led to the following conclusions. As the novel stochastic back-off concept takes the full information of the density

function into account, the optimization needs only a single iteration to converge. Thus, the simpler structure of the stochastic back-off approach results in lower computational demands than the conventional back-off approach. Moreover, we also demonstrated that polynomial chaos expansion in combination with the kernel density estimator is essential for deriving meaningful probability density functions at low computational costs. Compared with standard Monte Carlo simulations, the overall need for CPU-intensive reference simulations was reduced considerably, i.e., the stochastic back-off strategy is at least 20 times faster. In general, this strategy also scales well with large-scale process design problems with many uncertain model parameters based on the recent progress in highly efficient PCE routines, which we will analyze in more detail in future work.

Acknowledgement

X. Xie acknowledges funding from the "Promotionsprogramm μ-Props" by MWK Niedersachsen and the support from the International Max Planck Research School for Advanced Methods in Process and Systems Engineering, MPI Magdeburg.

References

Adamo, A., Beingessner, R.L., Behnam, M., Chen, J., Jamison, T.F., Jensen, K.F., Monbaliu, J.-C.M., Myerson, A.S., Revalor, E.M., Snead, D.R., et al., 2016. On-demand continuous-flow production of pharmaceuticals in a compact, reconfigurable system. Science 352 (6281), 61–67.

Aydin, E., Bonvin, D., Sundmacher, K., 2018. Nmpc using pontryaginâs minimum principle-application to a two-phase semi-batch hydroformylation reactor under uncertainty. Comput. Chem. Eng. 108, 47–56.

Bahri, P., Bandoni, J., Barton, G., Romagnoli, J., 1995. Back-off calculations in optimising control: a dynamic approach. Comput. Chem. Eng. 19, 699–708.

Bahri, P.A., Bandoni, J.A., Romagnoli, J.A., 1996. Effect of disturbances in optimizing control: steady-state open-loop backoff problem. AIChE J. 42 (4), 983–994.

Benyahia, B., Lakerveld, R., Barton, P.I., 2012. A plant-wide dynamic model of a continuous pharmaceutical process. Industr. Eng, Chem. Res. 51 (47), 15393–15412.

Blatman, G., Sudret, B., 2011. Adaptive sparse polynomial chaos expansion based on least angle regression. J. Comput. Phys. 230 (6), 2345–2367.

Botev, Z.I., Grotowski, J.F., Kroese, D.P., et al., 2010. Kernel density estimation via diffusion. Ann. Stat. 38 (5), 2916–2957.

Boukouvala, F., Niotis, V., Ramachandran, R., Muzzio, F.J., Ierapetritou, M.G., 2012. An integrated approach for dynamic flowsheet modeling and sensitivity analysis of a continuous tablet manufacturing process. Comput. Chem. Eng. 42, 30–47.

Cervera-Padrell, A.E., Skovby, T., Kiil, S., Gani, R., Gernaey, K.V., 2012. Active pharmaceutical ingredient (api) production involving continuous processes–a process system engineering (pse)-assisted design framework. Eur. J. Pharm. Biopharm. 82 (2), 437–456.

Diehl, M., Bock, H.G., Kostina, E., 2006. An approximation technique for robust nonlinear optimization. Math. Program 107 (1–2), 213–230.

Eder, R.J., Radl, S., Schmitt, E., Innerhofer, S., Maier, M., Gruber-Woelfler, H., Khinast, J.G., 2010. Continuously seeded, continuously operated tubular crystallizer for the production of active pharmaceutical ingredients. Crystal growth Design 10 (5), 2247–2257.

Efron, B., Hastie, T., Johnstone, I., Tibshirani, R., et al., 2004. Least angle regression. Ann. Stat. 32 (2), 407–499.

Emenike, V.N., Xie, X., Schenkendorf, R., Spiess, A.C., Krewer, U., 2019. Robust dynamic optimization of enzyme-catalyzed carboligation: a point estimate-based back-off approach. Comput. Chem. Eng. 121, 232–247.

Epanechnikov, V.A., 1969. Non-parametric estimation of a multivariate probability density. Theory Probab. Appl. 14 (1), 153–158.

Figueroa, J., Bahri, P., Bandoni, J., Romagnoli, J., 1996. Economic impact of disturbances and uncertain parameters in chemical processesâa dynamic back-off analysis. Comput. Chem. Eng. 20 (4), 453–461.

Galvanin, F., Barolo, M., Bezzo, F., Macchietto, S., 2010. A backoff strategy for model-based experiment design under parametric uncertainty. AIChE J. 56 (8), 2088–2102.

Gautschi, W., 2004. Orthogonal Polynomials: Computation and Approximation. Oxford University Press on Demand.

Gernaey, K.V., Cervera-Padrell, A.E., Woodley, J.M., 2012. A perspective on pse in pharmaceutical process development and innovation. Comput. Chem. Eng. 42, 15–29.

Gernaey, K.V., Gani, R., 2010. A model-based systems approach to pharmaceutical product-process design and analysis. Chem. Eng. Sci. 65 (21), 5757–5769.

ICH, 2005. Quality risk management q9. Guideline, ICH Harmonised Tripartite 4, 408.

Isukapalli, S., Roy, A., Georgopoulos, P., 1998. Stochastic response surface methods (srsms) for uncertainty propagation: application to environmental and biological systems. Risk Anal. 18 (3), 351–363.

Jolliffe, H.G., Gerogiorgis, D.I., 2015. Process modelling and simulation for continuous pharmaceutical manufacturing of ibuprofen. Chem. Eng. Res. Des. 97, 175–191.

Jolliffe, H.G., Gerogiorgis, D.I., 2016. Plantwide design and economic evaluation of two continuous pharmaceutical manufacturing (cpm) cases: ibuprofen and artemisinin. Comput. Chem. Eng. 91, 269–288.

Julier, S.J., Uhlmann, J.K., 2004. Unscented filtering and nonlinear estimation. Proc. IEEE 92 (3), 401–422.

Karunanithi, A.T., Achenie, L.E., Gani, R., 2006. A computer-aided molecular design framework for crystallization solvent design. Chem. Eng. Sci. 61 (4), 1247–1260.

Kim, K.-K.K., Braatz, R.D., 2013. Generalised polynomial chaos expansion approaches to approximate stochastic model predictive control. Int. J. Control 86 (8), 1324–1337.

Kim, K.-K.K., Shen, D.E., Nagy, Z.K., Braatz, R.D., 2013. Wiener'S polynomial chaos for the analysis and control of nonlinear dynamical systems with probabilistic uncertainties. IEEE Control Syst. 33 (5), 58–67.

Koller, R.W., Ricardez-Sandoval, L.A., Biegler, L.T., 2018. Stochastic back-off algorithm for simultaneous design, control, and scheduling of multiproduct systems under uncertainty. AIChE J.

Kookos, I.K., Perkins, J.D., 2016. Control structure selection based on economics: generalization of the back-off methodology. AIChE J. 62 (9), 3056–3064.

Kwon, J.S.-I., Nayhouse, M., Christofides, P.D., Orkoulas, G., 2013. Protein crystal shape and size control in batch crystallization: comparing model predictive control with conventional operating policies. Industr. Eng. Chem. Res. 53 (13), 5002–5014.

Lakerveld, R., Benyahia, B., Braatz, R.D., Barton, P.I., 2013. Model-based design of a plant-wide control strategy for a continuous pharmaceutical plant. AIChE J. 59 (10), 3671–3685.

Mandur, J., Budman, H., 2014. Robust optimization of chemical processes using bayesian description of parametric uncertainty. J. Process. Control 24 (2), 422–430.

Marelli, S., Sudret, B., 2015. Uqlab user manual polynomial chaos expansions. Chair of Risk, Safety & Uncertainty Quantification 1, 9–104.

Mascia, S., Heider, P.L., Zhang, H., Lakerveld, R., Benyahia, B., Barton, P.I., Braatz, R.D., Cooney, C.L., Evans, J.M., Jamison, T.F., et al., 2013. End-to-end continuous manufacturing of pharmaceuticals: integrated synthesis, purification, and final dosage formation. Angewandte Chemie 125 (47), 12585–12589.

Maußner, J., Freund, H., 2018. Efficient calculation of constraint back-offs for optimization under uncertainty: a case study on maleic anhydride synthesis. Chem. Eng. Sci. 192, 306–317.

Montes, F., Gernaey, K.V., Sin, G., 2018. Dynamic plantwide modeling, uncertainty and sensitivity analysis of a pharmaceutical upstream synthesis: ibuprofen case study. Industr. Eng. Chem. Res.

Nagy, Z., Braatz, R., 2007. Distributional uncertainty analysis using power series and polynomial chaos expansions. J. Process. Control 17 (3), 229–240.

Nagy, Z.K., 2009. Model based robust control approach for batch crystallization product design. Comput. chem. eng. 33 (10), 1685–1691.

Nagy, Z.K., Braatz, R.D., 2003. Worst-case and distributional robustness analysis of finite-time control trajectories for nonlinear distributed parameter systems. IEEE Trans. Control Syst. Technol. 11 (5), 694–704.

Nagy, Z.K., Braatz, R.D., 2004. Open-loop and closed-loop robust optimal control of batch processes using distributional and worst-case analysis. J. Process. Control 14 (4), 411–422.

Narraway, L.T., Perkins, J.D., 1993. Selection of process control structure based on linear dynamic economics. Industr. Eng. Chem. Res. 32 (11), 2681–2692.

Nayhouse, M., Tran, A., Kwon, J.S.-I., Crose, M., Orkoulas, G., Christofides, P.D., 2015. Modeling and control of ibuprofen crystal growth and size distribution. Chem. Eng. Sci. 134, 414–422.

Paulson, J.A., Mesbah, A., 2017. An efficient method for stochastic optimal control with joint chance constraints for nonlinear systems. Int. J. Robust Nonlinear Control.

Perkins, J., Gannavarapu, C., Barton, G., 1990. Choosing control structures based on economics. IEE Colloquium on Successful Industrial Applications of Multivariable Analysis 1, 1–3.

Qamar, S., Elsner, M., Angelov, I., Warnecke, G., Seidel-Morgenstern, A., 2006. A comparative study of high resolution schemes for solving population balances in crystallization. Comput. Chem. Eng. 30 (6–7), 1119–1131.

Rafiei, M., Ricardez-Sandoval, L.A., 2018. Stochastic back-off approach for integration of design and control under uncertainty. Industr. Eng. Chem. Res. 57 (12), 4351–4365.

Rafiei-Shishavan, M., Mehta, S., Ricardez-Sandoval, L.A., 2017. Simultaneous design and control under uncertainty: a back-off approach using power series expansions. Comput. Chem. Eng. 99, 66–81.

Rangavajhala, S., Mullur, A., Messac, A., 2007. The challenge of equality constraints in robust design optimization: examination and new approach. Struct. Multidiscip. Optim. 34 (5), 381–401.

Rashid, M.A., 2011. Crystallization engineering of ibuprofen for pharmaceutical formulation. PhD dissertation, Queensland University of Technology.

Rooney, W.C., Biegler, L.T., 2003. Optimal process design with model parameter uncertainty and process variability. AIChE J. 49 (2), 438–449.

Rossner, N., Heine, T., King, R., 2010. Quality-by-design using a gaussian mixture density approximation of biological uncertainties. IFAC Proceedings Volumes 43 (6), 7–12.

Saltelli, A., Ratto, M., Tarantola, S., Campolongo, F., 2005. Sensitivity analysis for chemical models. Chem. Rev. 105 (7), 2811–2828.

Savin, É., Faverjon, B., 2017. Computation of higher-order moments of generalized polynomial chaos expansions. Int. J. Numer. Methods Eng. 111 (12), 1192–1200.
Schenkendorf, R., Xie, X., Krewer, U., 2018a. An efficient polynomial chaos expansion strategy for active fault identification of chemical processes. Comput. Chem. Eng.
Schenkendorf, R., Xie, X., Rehbein, M., Scholl, S., Krewer, U., 2018b. The impact of global sensitivities and design measures in model-based optimal experimental design. Processes 6 (4), 27.
Shen, D.E., Braatz, R.D., 2016. Polynomial chaos-based robust design of systems with probabilistic uncertainties. AIChE J. 62 (9), 3310–3318.
Shi, J., Biegler, L.T., Hamdan, I., Wassick, J., 2016. Optimization of grade transitions in polyethylene solution polymerization process under uncertainty. Comput. Chem. Eng. 95, 260–279.
Simon, L.L., Pataki, H., Marosi, G., Meemken, F., Hungerbühler, K., Baiker, A., Tummala, S., Glennon, B., Kuentz, M., Steele, G., et al., 2015. Assessment of recent process analytical technology (pat) trends: a multiauthor review. Organic Process Res. Dev. 19 (1), 3–62.
Srinivasan, B., Bonvin, D., Visser, E., Palanki, S., 2003. Dynamic optimization of batch processes: ii. role of measurements in handling uncertainty. Comput. Chem. Eng. 27 (1), 27–44.
Su, Q., Benyahia, B., Nagy, Z.K., Rielly, C.D., 2015. Mathematical modeling, design, and optimization of a multisegment multiaddition plug-flow crystallizer for antisolvent crystallizations. Organic Process Res. Dev. 19 (12), 1859–1870.
Telen, D., Vallerio, M., Cabianca, L., Houska, B., Van Impe, J., Logist, F., 2015. Approximate robust optimization of nonlinear systems under parametric uncertainty and process noise. J. Process Control 33, 140–154.
Vervaet, C., Remon, J.P., 2005. Continuous granulation in the pharmaceutical industry. Chem. Eng. Sci. 60 (14), 3949–3957.
Visser, E., Srinivasan, B., Palanki, S., Bonvin, D., 2000. A feedback-based implementation scheme for batch process optimization. J. Process Control 10 (5), 399–410.
Xie, X., Krewer, U., Schenkendorf, R., 2018a. Robust optimization of dynamical systems with correlated random variables using the point estimate method. IFAC–PapersOnLine 51 (2), 427–432.
Xie, X., Schenkendorf, R., Krewer, U., 2017. Robust design of chemical processes based on a one-shot sparse polynomial chaos expansion concept. In: Computer Aided Chemical Engineering, Vol. 40. Elsevier, pp. 613–618.
Xie, X., Schenkendorf, R., Krewer, U., 2018b. Efficient sensitivity analysis and interpretation of parameter correlations in chemical engineering. Reliab. Eng. Syst. Saf.
Xiu, D., Karniadakis, G.E., 2002. The wiener–askey polynomial chaos for stochastic differential equations. SIAM J. Sci. Comput. 24 (2), 619–644.
Zhang, H., Lakerveld, R., Heider, P.L., Tao, M., Su, M., Testa, C.J., D'Antonio, A.N., Barton, P.I., Braatz, R.D., Trout, B.L., et al., 2014. Application of continuous crystallization in an integrated continuous pharmaceutical pilot plant. Crystal Growth Design 14 (5), 2148–2157.